Twenty-Sixth Symposium (International) on Combustion/The Combustion Institute, 1996/pp. 1181–1188

# TUNABLE DIODE LASER ABSORPTION MEASUREMENTS OF CARBON MONOXIDE AND TEMPERATURE IN A TIME-VARYING, METHANE/AIR, NON-PREMIXED FLAME

R. REED SKAGGS AND J. HOUSTON MILLER

*Department of Chemistry*
*The George Washington University*
*Washington, DC 20052, USA*

A time-varying, axi-symmetric, methane/air, nonpremixed flame is created by imposing a sinusoidal modulation to the fuel flow rate, which creates flames that "pinch off" and then detach from the burner. Carbon monoxide concentrations and temperatures are measured using tunable diode laser absorption spectroscopy (TDLAS) and are compared with those observed in a nonperturbed flame. The measurements indicate that at most phases of the oscillation, the time-varying flame is both broader and taller than the steady flame. Just before the flame detaches, high levels of CO are observed at the flame tip in regions of the flame that have high soot loading. In the detached flames, relatively high levels of CO remain and the time-averaged emission index for CO is larger in the oscillating flame.

## Introduction

Turbulent, nonpremixed combustion has attracted increased interest in recent years because of its application in a variety of practical combustors. Unfortunately, even with the best diagnostics it is not possible to obtain the quantity and quality of data with enough temporal resolution to fully characterize these systems. Further, it is not yet possible to numerically simulate the details of both complex chemistry and fluid mechanics that occur during turbulent combustion. During the past several years, significant progress in both the experimental data available and our ability to model combustion in steady-state, laminar, nonpremixed hydrocarbon flames, particularly those fueled by methane [1–3], has been made. This effort has been driven in part by the potential use of these data and models in flamelet modeling of turbulent combustion [4]. Between these two extremes, exists a third class of nonpremixed combustion: flickering or time-varying flames. The latter may be formed by imposing a periodic fluctuation to the fuel flow rate of a laminar flame. If the fuel flow perturbation is sufficiently large, the flames formed are exemplified by the formation of vortical structures. It has therefore been suggested [5–8] that time-varying flames offer an ideal environment to reproducibly study chemistry-turbulence interactions that are believed to control ignition, extinction, and flame propagation in turbulent reacting flows.

To date, much of the experimental efforts in nonsteady, low velocity, hydrocarbon diffusion flames have focused on using imaging techniques to study the temporal development of interactions between turbulence and flame chemistry. Experiments have been performed in acoustically forced flames by Gutmark et al. [9–11], who have imaged hydroxyl radicals in propane/air diffusion flames, and Vandsburger et al. [12,13] and Kim et al. [14] who used schlieren and $TiO_2$ imaging in methane/air and propane/air flames, respectively. Smyth et al. [5–7] and Cattolica and Vosen [15,16] have made laser-induced fluorescence (LIF) measurements of hydroxyl radicals in time-varying methane/air flames. Structural descriptions of nonsteady flames have been provided by Buckmaster and Peters [17], Hamins et al. [18], and Roquemore et al. [4,19] for gaseous diffusion flames, and Cetegen and Ahmed [20] for buoyant plumes and pool fires.

One of the key observations of Smyth et al. [5–7] has been that the peak soot volume fraction is enhanced by a factor of 5, and the time-averaged, volume-integrated soot levels increased by a factor of 4 for methane/air time-varying flames relative to those without acoustic perturbation. Further, flame "pinch off" was observed and the flame became broader with the flame width increasing as a function of the amplitude of the perturbation.

It is well established that emissions of soot and carbon monoxide are correlated [21–27]. For example, in laminar flames it has been observed that as the concentration of soot increases, the concentration of CO increases, while both the OH radical concentration and temperature decrease [21]. Because CO and soot are both oxidized by OH radicals under flame conditions [27–30] it has been suggested that soot and CO have a competitive relationship for OH radicals in hydrocarbon diffusion flames [21,22,25,28,30]. Puri and Santoro [21] found

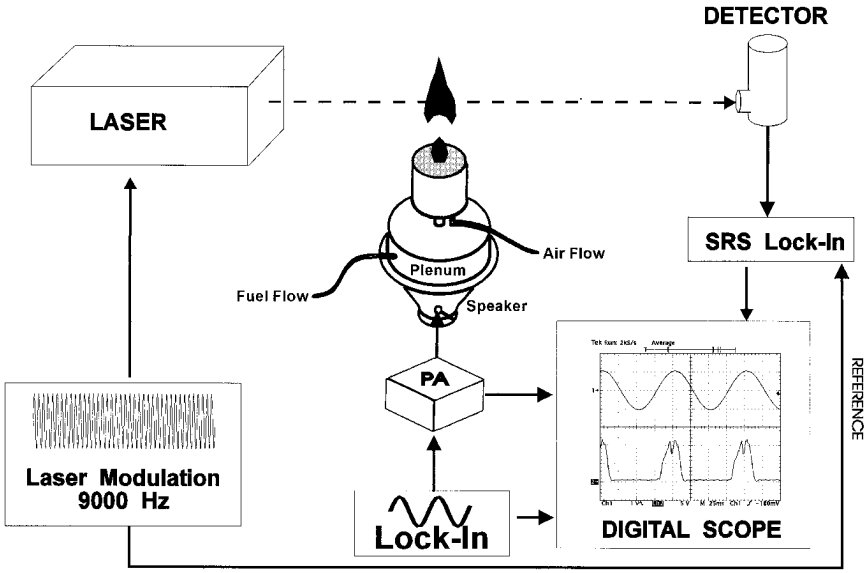


FIG. 1. Experimental configuration for TDLAS measurements of CO concentrations and temperatures in a methane/air, time-varying diffusion flame.

that increased amounts of soot result in larger concentrations of CO as well as depletion of OH radicals [25] at the flame tip in a series of methane flames that were doped with increased amounts of butane or butene to increase the sooting characteristics. Skaggs and Miller [30] found that soot oxidation, which forms CO, occurs at a faster rate than the rate of CO oxidation leading to a depletion of OH radicals in a series of ethylene flames near the smoke point.

Most of the previous measurements in time-varying flames have utilized ultraviolet and visible radiation to probe nonsteady combustion. In general, these techniques do not trivially provide quantitative measurements of species concentrations and suffer from some interferences in the presence of soot particles and/or polynuclear aromatic hydrocarbons (PAHs). For example, LIF of PAHs, which emit light in both the ultraviolet and visible spectral regions, interferes with OH radical and nitric oxide LIF measurements. In nonsteady flames, the use of invasive probes such as quartz microprobes or thermocouples is hampered by their relatively slow response time.

Tunable diode laser absorption spectroscopy (TDLAS) has been demonstrated to be a valuable probe for species' concentrations and temperatures even when the local soot level is high [30–39]. In this paper, we present a comparison of CO concentrations and temperatures observed with TDLAS in both a stable and time-varying, axi-symmetric, methane/air diffusion flames which have been previously investigated by Smyth et al. [5–7]. We will demonstrate that that both the maximum observed CO level in the flame, as well as the emission index for CO, are greater in the time-varying flame.

## Experimental

### *Time-Varying Flame Burner*

Figure 1 shows the experimental configuration used in this study. The flames investigated were supported on a modified axi-symmetric diffusion burner [40] whose design was adapted from the original developed by Smyth et al. [5–7] at the National Institute of Standards and Technology (NIST). The fuel flow velocity was modulated by passing the metered flow through a brass plenum (6″ inner diameter, 1″ in height) fitted with a diaphragm and 8″-loudspeaker (Radio Shack Model RS-1024). The burner apparatus is supported on a two-dimensional, computer-controlled positioning system.

Because of subtle differences in installation of the rubber diaphragm material, some care was required to match the conditions established by Smyth et al. [5–7]. In their work, they describe flames created with both a "0.75 V" and "1.5 V" forcing amplitude to the loudspeaker. By careful comparison of CCD images of both flame luminosity and OH LIF in our burner and in the NIST burner, we found that only a 0.275-V peak-to-peak excitation was required on our burner to create the "0.75 V" flame. In this paper, we have studied this "0.75 V," moderately flickering flame.

In the TDLAS experiments, the sine wave oscillation was provided by a lock-in amplifier (PAR model 5209) amplified by a PA (Radio Shack Model MPA 45) amplifier, and monitored at the loudspeaker (to account for voltage drop at the speaker) by a digital oscilloscope (Tektronix model TDS350) (see later).

The fuel used in this study was C.P. grade methane gas from Potomac Air Gas Company. The air supply was provided from an in-house compressor. The fuel flow rates were measured with a rotameter which was calibrated using a soap bubble technique. Air flow was monitored by a Hastings mass flow meter. Stabilization of the flames was aided by using a series of outer screens that surrounded the burner apparatus each with a 3 × 3-cm-square opening to allow for passage of the infrared beam.

### *Tunable Diode Laser Apparatus*

The experimental details of the TDLAS arrangement have been described previously [8,30,34] and only modifications for measurements in the time-varying system will be described here. The spectral output of a diode laser is coarsely determined by its composition and fine tuned by its temperature. The diode laser used for this study has a spectral output between 2110 and 2190 $cm^{-1}$ and was mounted in a closed-cycle helium refrigerator whose temperature is maintained with a cryogenic temperature stabilizer. Further refinements of temperature (and thus the laser's frequency) are possible by adjusting the injection current through the diode. In a typical experiment, the diode current was ramped up slowly to produce a spectral frequency scan of $\approx 0.85\ cm^{-1}$. In most experiments, a sinusoidal, 9000-Hz, small amplitude modulation was applied to the diode current. To correlate the current through the diode with the relative frequency of the spectral output, scans through a Ge etalon with a free spectral range of $\approx 0.048\ cm^{-1}$ were collected daily. Data collected in these etalon scans showed that a typical 0.02-A current sweep corresponds to a scan of $\approx 0.85\ cm^{-1}$. The emitted infrared light was collimated, directed through a mode-selection monochromator, passed through the flame, and finally focused onto a liquid-nitrogen-cooled InSb detector.

The detector signal was sent to a phase sensitive, lock-in amplifier (Stanford Research Systems [SRS] model SR850 DSP). The lock-in amplifier was set to sample the detector at twice the modulation frequency (2*f* detection) with an output time constant of 1 ms. To obtain temporal information from the time-varying absorption signal, the output signal from the SRS lock-in amplifier was directed to the second channel of the digital oscilloscope. At each location in the flame, the digital oscilloscope waveform was recorded at each spectral frequency as the diode injection current was scanned over the desired spectral range. Data were collected every 5 mm in height from 5 to 160 mm above the burner and every 0.8 mm radially from −24.8 to 24.8 relative to the burner centerline. The incident beam intensity, $I^\circ$, was acquired by collecting a nonmodulated spectrum before and after each height's data set.

### *Theoretical Background*

TDLAS is a line-of-sight technique where the absorption signal observed at the detector is the convolution of the incremental absorptions from each spatial location in the flame. In inhomogeneous flows, a tomographic reconstruction procedure must be employed to recover spatial information. The incremental absorptions also occur over short pathlengths in which the contribution from a given spatial region is small. Our experience in steady, axi-symmetric, methane/air [37,41] and ethylene/air diffusion flames [30] has allowed us to develop a reliable experimental technique for making these measurements that uses both wavelength modulation spectroscopy (WMS) [36,37,42,43] to enhance the detectability of weak signals and tomographic reconstruction [44] to recover spatial information.

It has been previously demonstrated [45–48] that the use of modulation techniques can increase the sensitivity of weak absorption signals. In these experiments, the magnitude of a detector signal which is sampled at twice the laser's modulation frequency, $x''$, is a function of temperature and concentration through [49,50]

$$x'' = F_2(v - v_0) \cdot S(T) \cdot g(v_0) \cdot P_j \cdot l \cdot I^\circ \qquad (1)$$

where $I^\circ$ is the incident laser intensity; $S$ is the temperature-dependent line strength for the transition; $g$ is the line shape factor evaluated at the line center; $P_j$ is the partial pressure of the absorbing species, and $l$ is the pathlength. Linestrength and lineshape values were obtained from the HITRAN [51] database at room temperature, and were recalculated for combustion conditions. $F_2$ is the second Fourier component of the modulated absorption coefficient [43], a function that looks qualitatively like the second derivative of the absorption feature [42]. In general, both collisional and Doppler broadening effects on line shapes must be considered in quantitative spectroscopy. However, Miller et al. [34] have demonstrated that under atmospheric pressure flame conditions, a Lorentzian profile function can be used to describe the experimental lineshape, $g$, and its second harmonic, $F_2$.

After data collection, a three-point Abel inversion algorithm [44] was employed to reconstruct the incremental absorption at each radial location in the flame for every frequency in the temporally resolved, line-of-sight spectra. The resulting data were then combined to build spectra for each radial and temporal location. All deconvolution techniques used in

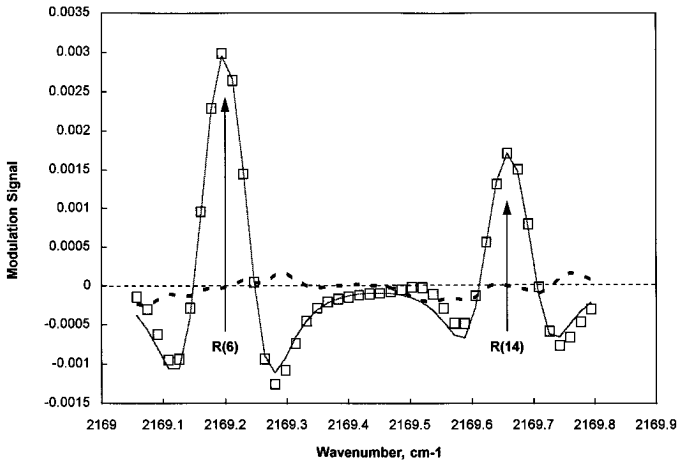


FIG. 2. Fit of reconstructed radial data (□) at positions of 15 mm above the fumes, 0.8 mm radial, and 75 ms. The solid line is the synthetic spectrum, and the residuals (experiment-calculated) are given by the dashed line. The two CO absorptions are the R(6) ($1 \leftarrow 0$) and R(14) ($2 \leftarrow 1$) lines, respectively.

tomography suffer from increased noise near the centerline, and even though the three-point Abel inversion is less sensitive to this effect than other techniques [44], we used a Savitzky-Golay [52] digital filter before and after the inversion to smooth data.

The radial (reconstructed) spectra were fit to equation 1 with three adjustable parameters: the partial pressure of CO, the local flame temperature, and the collisional halfwidth. Figure 2 shows a representative fit of a reconstructed spectrum located at 15 mm above the surface of the burner, a temporal location of 15 ms, and a radial position of 0.8 mm from the burner centerline. In this region of the infrared spectrum (near 2169 $cm^{-1}$), there are two significant absorption lines of carbon monoxide: the R(6) line of the vibrational fundamental band ($v' = 1 \leftarrow v'' = 0$) and the R(14) line of the first vibrational "hot band" ($v' = 2 \leftarrow v'' = 1$). Temperature and concentration data from the fits were obtained as a function of radial position and time, and these data were used to build three-dimensional concentration and temperature profiles for each profiled height.

In a final series of experiments, a 14-cm-diameter, 26.5-cm-tall brass chimney was placed around and over the burner. A glass plate with a 3.5-cm-diameter hole in its center rested on top of the chimney. The plate sat at approximately 17 cm above the top of the fuel tube. The CO emission index, defined as the mass of CO emitted divided by the mass of fuel consumed, was measured by making a series of CO TDLAS measurements above the glass plate exit hole, tomographically reconstructing the CO concentrations and calculating the integrated mass flow rate of CO from the burner. In these experiments, absorption signals were averaged over several flame modulation cycles.

As mentioned above, both in-flame and emission index data required tomographic reconstruction of data collected over short effective pathlengths. This greatly limits the sensitivity of the TDLAS technique. In the results presented below, we established a criteria for data quality by requiring data retained to have a signal-to-noise ratio in excess of 3. For this purpose, we define the "signal" as the magnitude of the $x''/I^0$ for the CO fundamental absorption, and the "noise" as the standard deviation of the spectral fit residuals. Even when satisfactory concentration data are available, temperature data may not be reliable because of nondetectability of the "hot band" (temperatures less than ≈800 K). For both flames studied, we established the uncertainty in CO measurements due to temperature uncertainties by performing spectral fits at peak CO locations where the temperatures were fixed 200 K higher and lower than that found in the original fits. This analysis demonstrated that the peak CO concentrations changed approximately ±1 mole percent for the corresponding temperature departure. Repeating this exercise at peak temperature locations, we found that a ±200 K deviation in temperature resulted in less than a mole percent change in CO concentrations.

## Results

### *Steady Flame Concentrations and Temperatures*

Figure 3 presents two contour plots of the experimentally measured concentrations and temperatures throughout the nonperturbed flame. The highest observed CO concentrations (0.03–0.04 mole fraction) occurred low in the flame toward the outer regions and near the centerline at ≈45 mm above the burner. At 45 mm, the highest CO concentration (0.0458 mole fraction) was observed. The temperature data exhibited similar structural trends with the peak temperatures occurring at radial positions outside the peak CO positions. The peak centerline temperature was ≈1900 K at 55 mm above the burner. Qualitatively, the temperature data

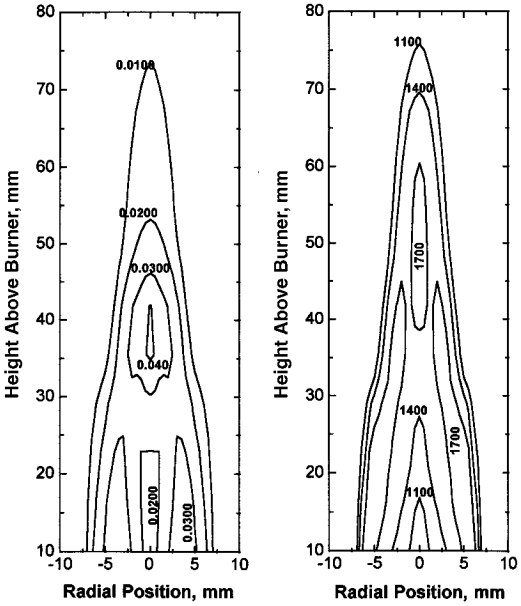


FIG. 3. Contour maps of CO concentrations and temperatures measured in the (79-mm) axi-symmetric, methane/air diffusion flame.

demonstrated trends similar to previously reported thermocouple temperature data of Richardson and Santoro [53]. The TDL measured peak temperatures at heights of 10, 30, and 50 mm above the burner are approximately 200 K lower than those observed by Richardson and Santoro [53], which is within the uncertainty of the TDLAS measurements near the flame front where the concentrations of CO are low.

*Time-Varying Flame: General Observations*

Figures 4 and 5 show "snap shots" of concentration and temperature contours at several phases. In our flame, we define time in reference to the 0-degree phase of the waveform imposed on the speaker and collected on the digital oscilloscope. In the NIST experiments [5–7], a different timing scheme was employed. Qualitatively, our data at 90 ms match the "30%" phase picture of OH and soot reported by NIST. Therefore, in the work reported here and for consistency with the NIST precedent, we consider the first part of the modulation cycle to begin at 70 ms which corresponds to the "10%" phase picture of OH and soot reported by NIST. In their observations [5–7], flame "pinch off" and broadening occurs when the fuel flow rate is perturbed. The pinched-off flame detaches at approximately 30–40 mm above the burner, which agrees with our observations.

*Concentrations*

The CO concentration profiles were contoured into five even levels from a threshold value of 100 ppm up to the maximum level of 0.07 mole fraction (i.e., 0.014 steps in mole fraction) as shown in Fig. 4. Elevated levels of CO (0.042–0.056 mole percent) were observed in the second half of the flame modulation cycle (20, 40, and 50 ms) in the annular region near the base of the flame. In the first half of the flame cycle, the flame appears to pinch toward the centerline, and relatively high CO levels are observed near the centerline at the flame "neck." At axial locations greater than 80 mm, the detached flame data is less structured and the concentrations are not as large as those observed lower in the flame. Also shown in Fig. 4 are OH LIF and soot particle scattering signals collected at NIST (from Ref. 6) at phases similar to those reported here. In the image labeled as 20 ms in Fig. 4 and again in that labeled 90 ms (equivalent to 60 and 30% phase, respectively, in the NIST work), high levels of CO are observed near the tip of the flame near the maximum of the soot scattering signal.

*Temperatures*

The temperature data were contoured in 280-K increments from 800 to 2200 K and are plotted in Fig. 5. They are structurally similar to the concentration data collected at the same temporal locations, although the distance between temperature maxima is greater. The lower limit corresponds to the approximate lowest temperature where the R(14) (2 $\leftarrow$ 1) absorption line could be observed. At 20 ms, consistent temperature data were observed from 5 to 25 mm above the burner and again from 85 to 95 mm. Low in the flame between 20 to 50 ms, the peak temperatures (1640–1920 K) occur near the perimeter of the flame and move toward the centerline with increasing height. At 80 mm and higher, the detached flame peak temperature contours appear broader than their counterparts lower in the flame. At 70 ms, the detached flame has almost progressed out of our observation region with the appearance of sparse data at 160 mm above the burner. At 45 mm above the burner at 90 ms, the flame width has broadened significantly with peak temperatures observed at a radial position of 11.2 mm from the centerline. In the steady flame, the distance between temperature maxima never exceeded $\approx$15 mm. It should be noted that gaps in the temperature contour do not necessarily imply cool temperatures; they may also indicate that insufficient CO was present to make a temperature determination (cf. 25–80 mm above the burner in the 20-ms frame).

## Discussion

In agreement with measurements at NIST, we find that both the temperature and concentration

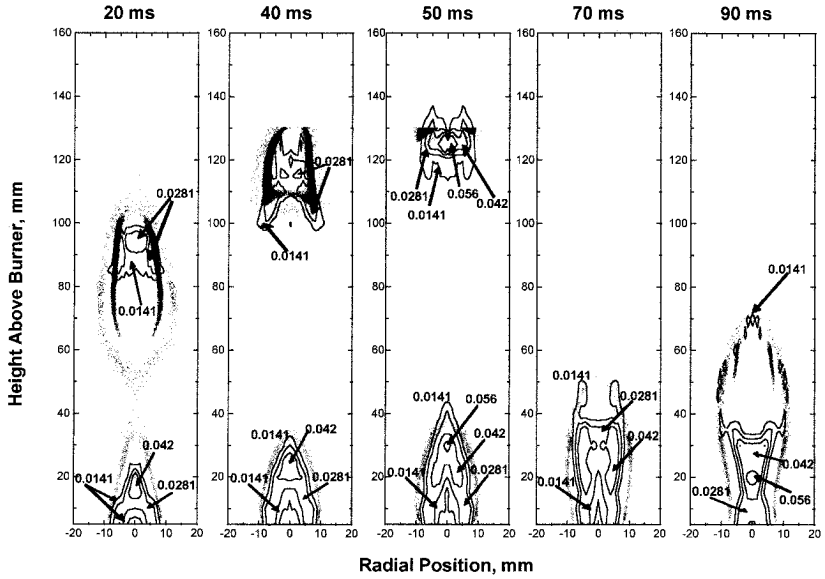


FIG. 4. Contour maps of concentrations measured in the time-varying, methane/air diffusion flame at temporal locations of 20, 40, 50, 70, and 90 ms. Also shown are OH LIF (lighter outer surface) and soot scattering signals (darker inner image) from NIST for similar phases [6]. It should also be noted that the OH/soot images are not available at heights above 128 mm.

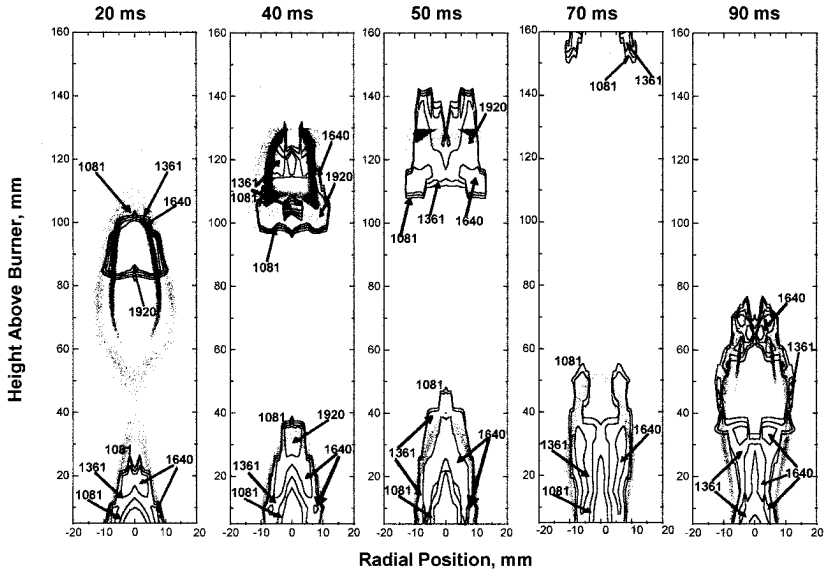


FIG. 5. Contour maps of temperatures measured in the time-varying, methane/air diffusion flame at temporal locations of 20, 40, 50, 70, and 90 ms. Also shown are OH/soot images (see Fig. 4).

profiles are broader than observed in the steady-state flame. At those times in which the flame has detached, the temperature and concentration profiles in the lower sections are qualitatively similar to the steady flame, although slightly higher CO levels are observed in the time-varying flame.

The observation of elevated CO concentrations in the time-varying flame may not be surprising: studies [54,55,56] of nonpremixed, turbulent, methane jet flames have shown CO concentrations that were higher than those predicted by steady, laminar, methane flame models. Barlow and Chen [54] performed a series of flamelet calculations to investigate the physical mechanism responsible for "nonflamelet" behavior that has been observed in turbulent flames and concluded that there are two possibilities for this phenomenon. First, a reduction in the degree of differential diffusion relative to a laminar flame can contribute to measurements of higher concentrations of combustion intermediates. Second, a steep decrease in scalar dissipation can cause the mass fractions of several intermediate species to overshoot their steady-state values. In another study, Masri et al. [55] measured peak CO mass fractions of $\approx 0.08$ in lower regions of turbulent, non premixed methane flames near extinction. Finally, Gore et al. [56] reported state relationships for CO in large-scale natural gas flames showing peak CO levels of almost 6 mole percent appearing just rich of the stoichiometric surface.

It is also noteworthy that the CO levels near the flame tip in the pinched flame and in the detached flame are high and these high levels occur where soot concentrations are also high. In these flame regions, soot oxidation is expected to occur, a process whose products include CO [30].

The fact that CO is observed with slightly higher concentrations over a far broader region of space clearly suggests that there is more CO in the time varying flame, and the possibility for greater CO emission exists. In fact, our time-averaged emission index measurements show that there are 8.1 mg of CO emitted for every gram of methane consumed in the time-varying flame. For comparison, the emission index in the steady flame was 1.6 mg CO/1 g $CH_4$. Perhaps coincidentally, the factor of 5 between these two values is the approximate enhancement in peak soot volume fraction observed by Smyth et al. [5–7] between the two flames.

## Conclusions

Spatially and temporally resolved measurements of temperature and CO concentrations were made in both steady-state and time-varying, nonpremixed, methane/air flames. Although the peak levels of CO observed were only slightly greater in the time-varying flame, the spatial extent of CO, and thus its expected integrated level, was substantially greater in the time-varying flame. The emission index for CO was also greater in the time-varying flame, suggesting a link between enhanced soot loading and CO emission from flickering flames.

*Acknowledgments*

The authors would like to thank K. C. Smyth, D. A. Everest (NIST), and C. R. Shaddix (SANDIA) for their assistance in burner design and in establishing flame conditions. The authors would also like express their gratitude to J. Prelgo and D. Weiss for their assistance in data collection and analysis. Finally, this work was supported by Gas Research Institute contract 5093-260-2676 under the technical direction of Dr. Robert Serauskus.

## REFERENCES

1. Norton, T. S., Smyth, K. C., Miller, J. H., and Smooke, M. D., *Combust. Sci. Technol.* 90:1–34 (1993).
2. Bilger, R. W., Starner, S. H., and Kee, R. J., *Combust. Flame* 80:135 (1990).
3. Puri, I. K., Seshadri, K., Smooke, M. D., and Keyes, D. E., *Combust. Sci. Technol.* 56:1–22 (1987).
4. Davis, R. W., Moore, E. F., Roquemore, W. M., Chen, L. D., Vilimpoc, V., and Goss, L. P., *Combust. Flame* 83:263–270 (1991).
5. Smyth, K. C., Harrington, J. E., Johnsson, E. L., and Pitts, W. M., *Combust. Flame* 95:229–239 (1993).
6. Shaddix, C. R., Harrington, J. E., and Smyth, K. C., *Combust Flame* 99:723 (1994).
7. Shaddix, C. R. and Smyth, K. C., *Chem. Phys. Process. Combust.* 329 (1994).
8. Skaggs, R. R. and Miller, J. H., *Chem. Phys. Process. Combust.* 172 (1994).
9. Gutmark, E., Parr, T. P., Parr, D. M., and Schadow, K. C., *Twenty-Second (International) Symposium on Combustion,* The Combustion Institute, Pittsburgh, 1988, p. 523.
10. Gutmark, E., Parr, T. P., Parr, D. M., and Schadow, K. C., *J. Heat Transfer* 111:148–155 (1989).
11. Gutmark, E., Parr, T. P., Parr, D. M., and Schadow, K. C., *Combust. Sci. Technol.* 66:107–126 (1989).
12. Vandsburger, U., Seitzman, J. M., and Hanson, R. K., *Combust. Sci. Technol.* 59:455–461 (1988).
13. Lewis, G. S., Cantwell, B. J., Vandsburger, U., and Bowman, C. T., *Twenty-Second (International) Symposium on Combustion,* The Combustion Institute, Pittsburgh, 1988, pp. 515–522.
14. Kim, T. K., Park, J., and Shin, H. D., *Combust. Sci. Technol.* 89:83–100 (1993).
15. Cattolica, R. J. and Vosen, S. R., *Twentieth (International) Symposium on Combustion,* The Combustion Institute, Pittsburgh, 1984, p. 1273.
16. Cattolica, R. J. and Vosen, S. R., *Combust. Sci. Technol.* 48:77–87 (1986).
17. Buckmaster, J. and Peters, N., *Twenty-First*

*(International) Symposium on Combustion,* The Combustion Institute, Pittsburgh, 1986, pp. 1829–1836.
18. Hamins, A., Yang, J. C., and Kashiwagi, T., *Twenty-Fourth (International) Symposium on Combustion,* The Combustion Institute, Pittsburgh, 1992, pp. 1695–1702.
19. Chen, L. -D., Seaba, J. P., Roquemore, W. M., and Goss, L. P., *Twenty-Second (International) Symposium on Combustion,* The Combustion Institute, Pittsburgh, 1988, pp. 677–684.
20. Cetegen, B. M. and Ahmed, T. A., *Combust. Flame* 93:61–76 (1991).
21. Puri, R. and Santoro, R. J., *Fire Safety Science, Proceedings of the Third International Symposium,* (Langford, B. and Cox, G., Eds.) Elsevier, New York, 1991, pp. 595–604.
22. Puri, R., Moser, M., Santoro, R. J., and Smyth, K. C., *Twenty-Fourth Symposium (International) on Combustion,* The Combustion Institute, Pittsburgh, 1992, pp. 1015–1022.
23. Fischer, S. J. and Grosshandler, W. L. *Twenty-Second Symposium (International) on Combustion,* The Combustion Institute, Pittsburgh, 1988, pp. 1241–1249.
24. McCaffrey, B. J. and M. Harkleroad, *Twenty-Second Symposium (International) on Combustion,* The Combustion Institute, Pittsburgh, 1984, pp. 1555–1566.
25. Puri, R., Santoro, R. J., and Smyth, K. C., *Combust. Flame* 97:125–144 (1994).
26. Köylu, U. O. and Faeth, G. M. *Combust. Flame* 87:61–76 (1991).
27. Neoh, K. G., Howard, J. B., and Sarofim, A. F., in *Particulate Carbon Formation During Combustion,* D. C. Siegla, and G. W. Smith (Eds.), Plenum, New York, 1981, p. 261.
28. Fristrom, R. M. and Westenberg, A. A., *Flame Structure,* McGraw Hill, New York, 1965.
29. Neoh, K. G., J. B. Howard, and A. F. Sarofim, *Twentieth Symposium (International) on Combustion,* The Combustion Institute, Pittsburgh, 1985, p. 951.
30. Skaggs, R. R. and Miller, J. H., *Combust. Flame* 100:430–439 (1995).
31. Hanson, R. K., *Appl. Opt.* 19:482–484 (1980).
32. Varghese, P. L. and Hanson, R. K., *J. Quant. Spectrosc. Radiat. Transfer* 24:479–489 (1980).
33. Schoenung, S. M. and Hanson, R. K. *Combust. Sci. Technol.* 24:227–237 (1981).
34. Miller, J. H., Elreedy, S., Ahvazi, B., Woldu, F., and Hassanzadeh, P., *Appl. Opt.* 32:6082–6089 (1993).
35. Nguyen, Q. V., Dibble, R. W., Hofmann, D., and Kampmann, S., *Ber. Bunsenges. Phys. Chem.* 97(12) (1993).
36. Ouyang, X., Varghese, P. L., and Howell, J. R., "Tomographic Absorption Spectroscopy of Combustion Gases Using Tunable Infrared Diode Lasers," SPIE Conference on Environmental and Process Monitoring Technologies, 1992, Paper 1637-20.
37. Tolocka, M. P. and Miller, J. H., *Microchem. J.* 50:397–412 (1994).
38. Skaggs, R. R., Tolocka, M. T., and Miller, J. H., *Combust. Sci. Technol.,* 116–117(1-6):399 (1996).
39. Nguyen, Q. V., Edgar, B. L., Dibble, R. W., and Gulati, A., *Combust. Flame* 100:395–407 (1995).
40. Santoro, R. J., Yeh, T. T., Horvath, J. J., and Semerjian, H. G., *Combust. Sci. Technol.* 53:89–115 (1987).
41. Skaggs, R. R., Le, K. N., Miller, J. H., Honnery, D. R., and Kent, J. H., *Chem. Phys. Process Combust.* 167 (1993).
42. Arndt, R., *J. Appl. Phys.* 36:2522–2524 (1965).
43. Reid, J. and Labrie, D., *Appl. Phys. B* 26:203–210 (1981).
44. Dasch, C. J., *Appl. Opt.* 29:4884–4890 (1990).
45. Cassidy, D. T. and Reid, *J. Appl. Opt.* 21:1186–1190 (1982).
46. Slemr, F., Harris, G. W., Hastie, D. R., Mackay, G. I., and Schiff, H. J. *J. Geophys. Res.* 91:5371–5378 (1986).
47. Bruce, D. M. and Cassidy, D. T., *Appl. Opt.* 29:1327–1332 (1990).
48. Silver, J. A., *Appl. Opt.* 31:707–717 (1992).
49. Hanson, R. K., Varghese, P. L., and Schoenung, S. M., *Laser Probes for Combustion Chemistry,* ACS Symposium Series No. 134, (Crosley, D. R., Ed.), The American Chemical Society, Washington, DC, 1980, pp. 413–426.
50. Hanson, R. K. and Falcone, P. K., *Appl. Opt.* 17:2477–2480 (1978).
51. HITRAN database of infrared transition data. United States Air Force Geophysics Laboratory, 1992 edition.
52. Savitzky, A. and Golay, M. J. E., *Anal. Chem.* 36:1627 (1964).
53. Richardson, T. F. and Santoro, R. J., private communication, 1993.
54. Barlow, R. S., Chen, J. -Y., *Twenty-Fourth Symposium (International) on Combustion,* The Combustion Institute, Pittsburgh, 1992, pp. 231–237.
55. Masri, A. R., Bilger, R. W., Dibble, R. W., *Combust. Flame* 73:261–285 (1988).
56. Gore, J. P., Faeth, G. M., Evans, D., and Pfenning, D. B., *Fire Materials* 10:161–169 (1986).